Microstructure Changes in Sn-3.5Ag Solder Alloy during Creep

V.I. IGOSHEV,[1] J.I. KLEIMAN,[1] D. SHANGGUAN,[2] C. LOCK,[3] S. WONG,[3] and M. WISEMAN[3]

1.—Integrity Testing Laboratory Inc., 4925 Dufferin St., North York, M3H 5T6, Ont., Canada. 2.—Visteon Automotive Systems, Dearborn, Ml 48121. 3.—Visteon Automotive Systems, Markham, Ont., Canada

Experimental data on behavior of the Sn-3.5Ag solder alloy microstructure during tensile creep deformation and subsequent failure is described. Depending upon applied stress, the nucleation and further development of grain boundary defects that start at an earlier stage in the deformation process was revealed. A discussion is presented on possible micromechanisms of the crack formation process.

Key words: Crack formation, solder microstructure, tensile creep deformation

INTRODUCTION

Pb-free solder alloys are intended to completely substitute for traditional Pb-Sn compositions in conventional processes in the future.[1] It is very important, therefore, to understand the mechanical properties and behavior of such alloys that will allow one to predict the reliability in terms of lifetime of solder joints in assemblies. Creep is the most common and important micromechanical deformation mechanism of solder joints.[1] Due to a gap existing in the experimental database relevant to accelerated creep testing of Pb-free solders, it is not possible, presently, to make predictions with regard to solder joints' reliability.[2] It is not very clear whether their lifetime during accelerated creep testing is controlled by dislocation movement alone, or some other mechanisms play roles as well.

The analysis of experimental data on steady-state creep deformation of a number of Pb-free solder alloys has revealed that taking into account only the process of dislocation-based creep leads to a discrepancy between experimental and expected from theoretical considerations values of creep activation energy. To explain this discrepancy, it was suggested[2] that the process of grain boundary micro-fracture should be taken into account as well. The nucleation and subsequent growth of defects like pores and cracks that occur even during steady-state creep and well in advance of the final failure may explain the found discrepancy. Experimental data and microstructural observations obtained for Sn-3.5Ag solder alloy are presented in this paper in support of that theory.

(Received January 27, 1998 accepted August 7, 1998)

EXPERIMENTAL PROCEDURE

Ingots of commercial Sn-3.5Ag eutectic solder alloy were melted, and flat dog bone-shaped specimens (1.0 mm thick, 8.0 mm wide, 70 mm long; 2.0 mm wide and 15 mm long gage section) were cast in an aluminum mold at 523K and cooled in air for two hours.

Before testing, one surface of the specimen was mechanically polished. In order to avoid introducing initial damage, the specimens were placed in a specially designed holder during the polishing. Final polishing was done with 1 μm diamond paste. Marker lines 0.6–2.0 mm apart (measured before mechanical testing was initiated) were introduced on the polished surfaces of some specimens in the gage section normal to the loading direction using a Vickers's indenter under zero applied load. The lines provided an opportunity to measure the value and assess the uniformity of macroscopic plastic deformation (in terms of elongation) with an accuracy of 0.2%. For such measurements, the creep experiment was interrupted, the sample was taken out, and the distance between the marker lines was measured using an optical microscope. All specimens were aged at 373K for 100 h in silicon oil prior to the beginning of the experiment. To reveal the microstructure, the specimens were etched with 2%HNO_3-5%HCl-93% methyl alcohol solution for several seconds.

Creep tests under constant tensile load were carried out at (353.0 ± 0.1)K and (373.0 ± 0.1)K, that correspond to the homologous temperatures of η = (T/

T_m) = 0.714 and η = 0.755, respectively, where T_m is the alloy's melting point. Two initial stresses (10.00 and 11.25 MPa) were employed at 353K, whereas four initial stresses (7.50, 8.25, 10.00, and 11.25 MPa) were employed at 373K. These correspond to the normalized stress range of $\sigma/E = (2.2–3.3) \times 10^{-4}$, where E = 35 GPa and E = 33.6 GPa are the Young's modulus of Sn-3.5Ag alloy at 353 and 373K, respectively.[3] Vickers's microhardness of the solder was measured using a 25 g load applied for 15 s.

The microstructure, the fracture surfaces of specimens, and the elemental composition were evaluated using optical microscopy, scanning electron microscopy (SEM) (JEOL-T300) (secondary and backscattered electron detectors), and energy dispersive spectroscopy (URSA).

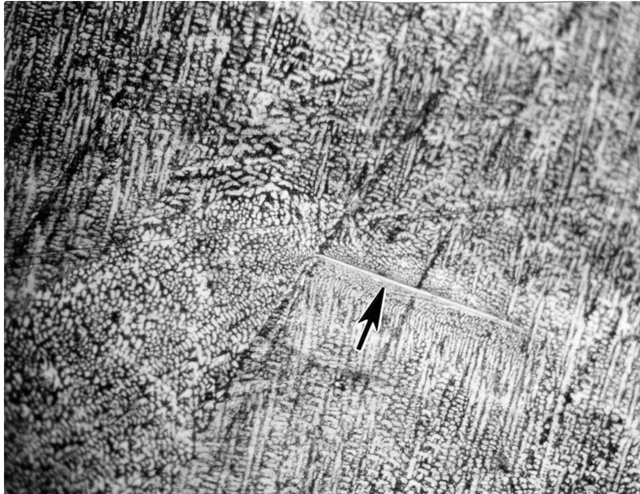

Fig. 1. Rod-like intermetallics of Ag_3Sn in the matrix of Sn. Annealing for 100 h at 373K. Optical microscopy, x160.

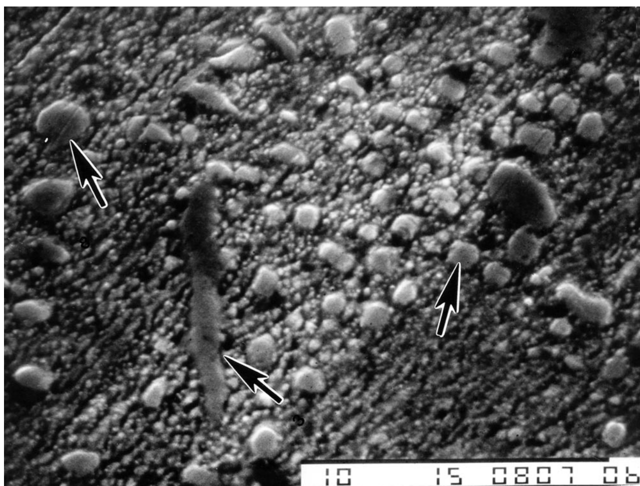

Fig. 2. Scanning electron microscopy (secondary electron image) of particles of Ag_3Sn intermetallics (marked with arrows) finely dispersed in the Sn matrix after annealing for 100 h at 373K, x 5000.

EXPERIMENTAL RESULTS

Initial Microstructure

The cooling rate for specimens after molding was expected to be low due to the large mass of the mold and the chosen method of cooling in air. Low cooling rates should cause formation of rod-like Ag_3Sn intermetallics in an essentially pure Sn matrix, while high cooling rates lead to formation of small (~1 μm) intermetallic particles dispersed in a Sn matrix.[3–5] Figure 1 shows a typical microstructure for the molded and aged specimens. This type of microstructure is in accord with the reported data for low cooling rates.[4] The microhardness value of HV = 13.8 ± 0.4, measured for one of the samples, was foumd to correspond closely to the value of HV= 13–14 reported for the same type of microstructure.[4] It should be noted, however, that microstructures obtained in our experiments with low cooling rates contained not only rod-like, but also finely dispersed particles of Ag_3Sn intermetallics in the Sn matrix as well (Fig. 2).

Microstructure During Creep

The microstructure of samples caused to creep was found to change depending on the applied stress. Two different changes to microstructure during creep deformation were identified. The first was associated with the stress range σ = (8.75–11.25) MPa, whereas the second was obtained at σ = 7.5 MPa.

The main features in the microstructural changes at higher stresses can be associated with defects (such as surface steps, pores, and microcracks) accumulating at grain boundaries (GB) and the matrix/interme-

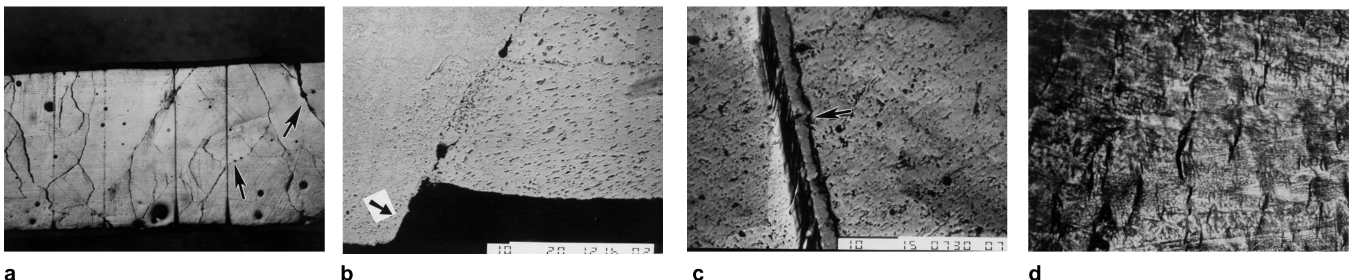

Fig. 3. Different types of surface damages occurring during creep deformation. (a) applied stress, σ = 10.00 MPa, temperature, T = 373K, testing time, τ = 24 h. GB micro-voids and a crack are marked with arrows. Optical microscopy, x25; (b) applied stress, σ = 10.00 MPa, temperature, T = 353K, testing time, τ = 60 h. Surface step at a GB is marked with an arrow. Cross-sectional backscattering compositional SEM image, x750; (c) applied stress, σ = 8.75 MPa, temperature, T = 373K, testing time, τ = 60 h. Ag_3Sn intermetallics rod protruding from the surface. Backscattering compositional SEM image, x2000; and (d) applied stress, σ = 7.50 MPa, temperature, T = 373K, testing time, τ = 360 h. Surface morphology after creep. Optical microscopy, x160.

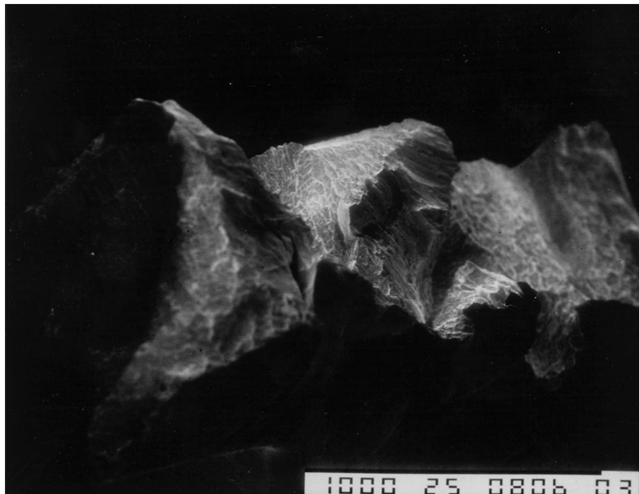

a

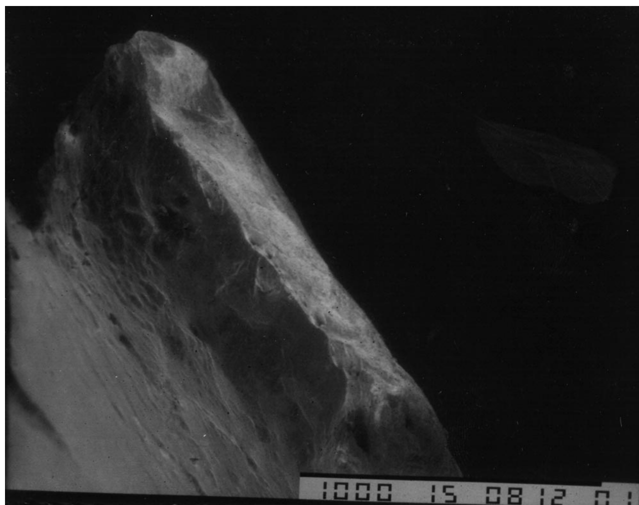

b

Fig. 4. Temperature, T = 373K. (a) brittle intercrystalline failure after creep at σ = 10.00 MPa, for 40 h. Secondary electron microscopy image, x 50; (b) secondary electrons image of ductile transcrystalline failure after creep at σ =7.50 MPa, for 410 h, x 50.

tallics interface (MII) (Fig. 3a–3c). It was found that the number of GB undergoing such changes depends on the applied stress. At the stress $\sigma = 8.75$ MPa, only a few GB were found to be affected at the fracture point. However, at $\sigma = 11.25$ MPa, the majority of GB and MII were affected (Fig. 3a). Analyzing Fig. 3, it can be suggested that defect accumulation is due to a grain and phase boundary sliding (GBS) process. This leads to formation of steps between the grains (marked with arrows in Fig. 3b) as well as between the matrix and rod-like intermetallics (marked with an arrow in Fig. 3c). A number of microvoids and cracks formed at GB (marked with arrows in Fig. 3b) can be seen as well. Similar changes were also observed after a testing time of only $\tau = 0.2\ \tau_c$, where τ_c is the specimen lifetime. They became more pronounced as the time increased. The samples ultimately failed via intercrystalline failure mode (Fig. 4a).

Samples conditioned at the lowest stress of $\sigma = 7.50$ MPa demonstrated “wavelike” features in their fractures, with no traces of GBS (Fig. 3d). The final

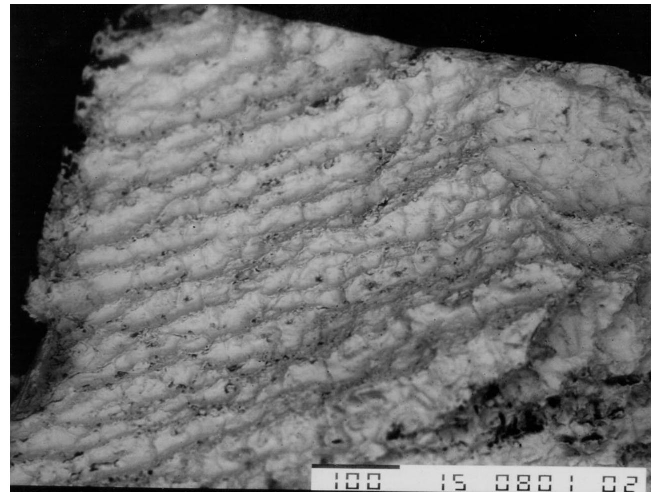

a

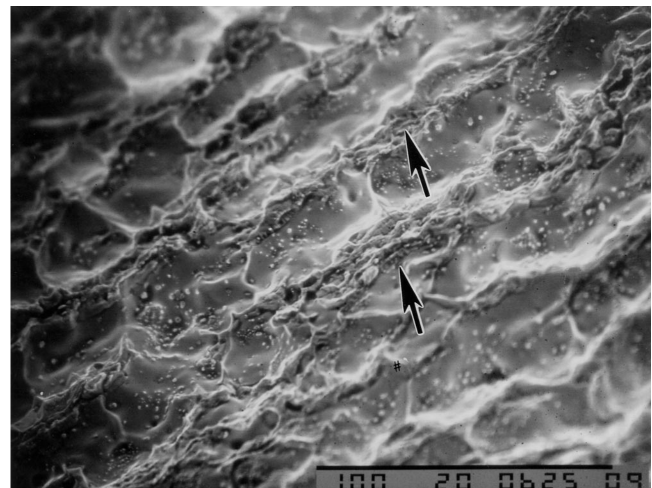

b

Fig. 5. Magnified images of an intercrystalline fracture zone, σ = 8.75MPa, temperature, T = 373K, τ_c = 120 h. (a) parallel striations, generated during creep. Backscattering compositional SEM image, x 150, and (b) striations and GB facets with particles of Ag_3Sn intermetallics. Secondary electron microscopy image, x 500.

fracture was ductile and was accompanied by considerable necking (Fig. 4b).

Fractography

Two different types of fracture surfaces were revealed. Fractures produced at the lowest applied stresses (7.50 MPa) did not exhibit any significant features and were representative of typical ductile transcrystalline failure. A typical example of fractures obtained at higher loads is shown in Fig. 5 that can be classified as intercrystalline. Small facets and parallel striations on grain surface can be seen in Fig. 5. The distance between striations was estimated at 25 μm and seemed to decrease with an increase in the applied stress.[a] Further SEM analysis of the GB facets (Fig. 5b and Fig. 6) indicated at a number of features:

- The striations (marked with the arrows in Fig.5b) that are typical of a ductile failure;
- The GB facets are flat, do not have any signs of

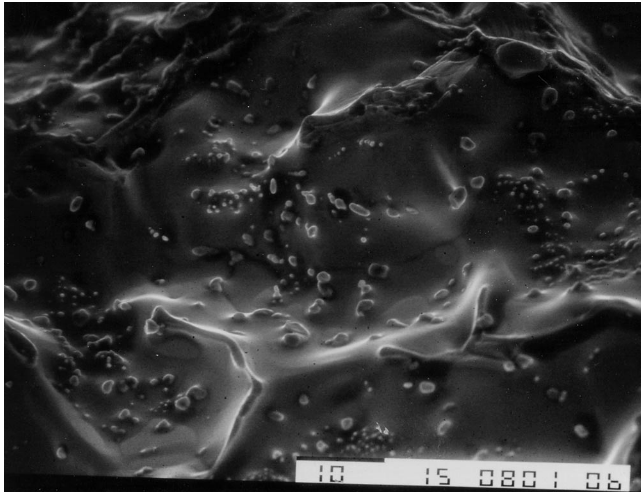

a

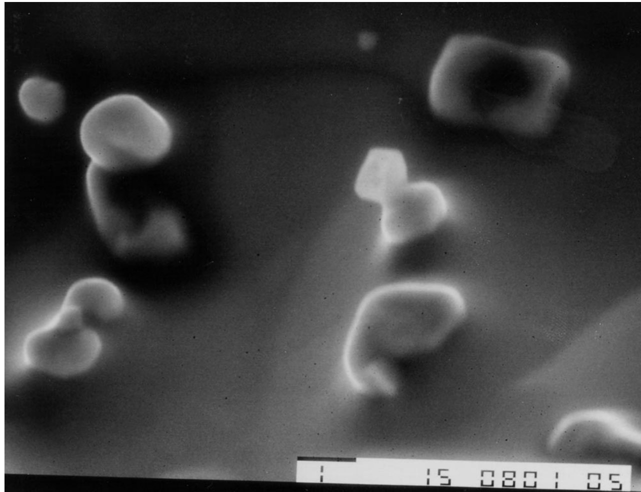

b

Fig. 6. Enlarged secondary electron SEM images of Fig. 5b showing particles of intermetallics protruding from the fracture surface: (a) x 1500, and (b) x 10000.

plastic deformation (Fig. 6a), and contain small, protruding particles of Ag_3Sn intermetallics (Fig. 6b), as established by energy dispersive spectroscopy (EDS) microprobe analysis.

SEM analysis of matching fracture surfaces indicated that both surfaces contained protruding particles. No cavities that can be associated with a pullout mechanism of the particles were evident in the analyzed samples.

Creep Data

Figure 7 presents the dependence of the lifetime data (τ_c) on the applied stress as obtained from a number of experiments at two different temperatures. Each point on the graph represents an average of 3–5 experiments. Analyzing the fractography data,

[a]The distance between the striations may be a very important microstructural parameter containing information on fracture micromechanism. In order to obtain the exact value of that parameter, geometric factors such as the orientation of fracture path and the viewing angle in the microscope (see. Fig. 4a) should be taken into consideration.

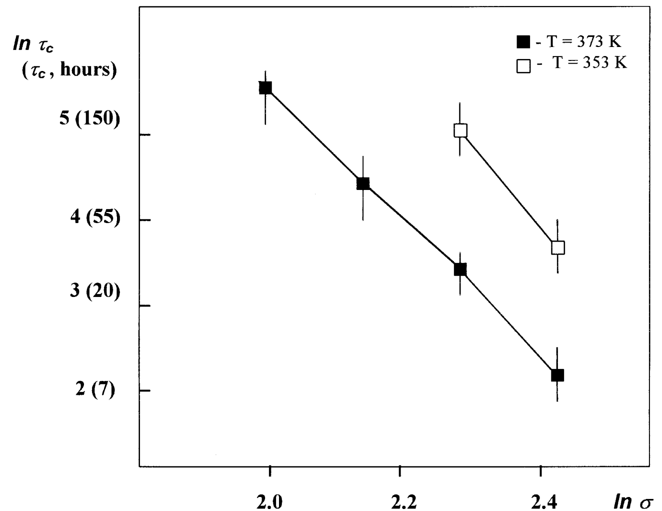

Fig. 7. Dependence of specimen lifetime τ_c vs the applied creep stress σ.

a change in the mode of fracture around the stress value of σ = 7.50 MPa can be suggested which is indicative of a change in the failure mechanism. Such phenomena should lead to a different stress exponent value n in the equation $\tau_c \sim \sigma^{-n}$ and consequently to a different line slope in the $\ln\tau_c$-$\ln\sigma$ plot in Fig. 7. More data of this type should, therefore, be accumulated, to resolve this ambiguity.

It should be noted that the measurement of the elongation, ε, calculated as the distance change between two marker lines, was very nonuniform along the specimen's length, and proved to be of little use in the process of generating the creep curves, at least for the chosen test conditions. The elongation value varied in the range of ε = (0–4.2)% depending just on the location of and initial distance between the marker lines, being independent on the stress and, consequently, did not reflect actual accumulated deformation. For instance, at the highest stress of σ = 11.25 MPa, the deformation accumulated at failure point was ε_c = 0.92%, for a stress σ = 10.00 MPa it was ε_c = 4.2%, and at σ = 8.75 MPa, ε_c = 0% was obtained.

DISCUSSION

The main objective in the discussed above experiments was to establish the nature of microstructural changes happening during creep deformation. Experimental data described above indicates that the changes occur as a process of accumulation of GB defects, starting at an earlier stage of creep and lasting for at least 70–80% of the specimen's lifetime.

Depending upon applied stress, two different types of fractures, namely transcrystalline at the lower applied stress, and intercrystalline at higher stresses were identified. The change in fracture surface appearance from trans- to intercrystalline, obviously points to a change in the creep micromechanism that controls the fracture process.

According to our data, at homologous temperatures η = 0.714 and η = 0.755, the specimen's lifetime is controlled by dislocation creep at normalized stresses

below $\sigma/E = 2.6 \times 10^{-4}$ (there is no GB cracking and the final failure is transcrystalline). The kinetics of GB cracking controls the specimen's lifetime above $\sigma/E = 2.6 \times 10^{-4}$ (the final failure is intercrystalline).

To discuss the nature of the micromechanism controlling the creep lifetime, three major observations can be summarized as follows:

- The striations on an intercrystalline fracture surface can be associated with a ductile failure path;
- The absence of any signs of plastic deformation on the GB facets indicates that a high temperature process of diffusive mass transport is responsible for their formation;
- GB facets contain small particles of Ag_3Sn intermetallics protruding from the matching fracture surfaces. Absence of cavities that should be left behind pulled-out particles during fracture means that during the creep the intermetallics particles failed also.

It is reasonable to suggest that the observed striations are due to dislocation pileup inside grain's slip bands that stopped at GB, i.e., with the GB acting as strong barriers for dislocation movement.[6] Usually, local stress concentrations caused by the pile-up can be accommodated by a grain boundary sliding process, particularly at high temperature. However, the presence of particles of hard intermetallic inclusions at GB in the Sn-3.5Ag alloy did not allow for the process of stress concentration relaxation by GBS mechanism.

Let us assume that due to such stress concentration around the dislocation pile-up, a failure (microcrack/void nucleation) of the nearest small particle of GB's intermetallics occurs.[b] Once created, such a defect serves as a vacancy sink in the process of stress relaxation. It grows by diffusive mass transport along GB. The driving force of that kinetic process is a permanent local stress concentration sustained by a continuous creep deformation inside the grain.[c] As the defect grows, the GB displacement becomes possible that, in turn, leads to the formation of steps on the surface. The final failure occurs when the defect size becomes roughly equal to the distance between slip bands where all plastic deformation had accumulated, and occurs by their ductile necking. The fracture surface produced during such a process will resemble one presented in Fig. 5 and Fig. 6.

An analysis of calculated activation energy values in steady-state creep studies of Sn-3.5Ag and a few other Pb-free solder alloys[2] revealed a considerable discrepancy between that data and expected values, assuming the process of dislocation movement is the only creep mechanism. To account for this discrepancy, it was suggested[2] that one of its origins is associated with the processes of GB failure that start already during the second (steady-state) creep stage. In such a case, these processes affect the steady-state creep-rate data, and the calculated activation energy is the apparent, and not the true value.

The initial experimental results for the Sn-3.5Ag solder alloy obtained for the applied stress range above $\sigma = 8.75$ MPa (that corresponds to normalized stress $\sigma/E = 2.6 \times 10^{-4}$)[d] support the above suggestion, at least for this alloy.[e] It is, therefore, conceivable to suggest that the process of accumulation of GB defects can explain the discrepancy between the experimental data and the expected values of creep activation energy reported.[3,4]

CONCLUSION

Preliminary experimental data on creep behavior of Sn-3.5% Ag alloy described in this paper allows to suggest that the creep process of Pb-free solder alloys, and particularly of Sn-3.5Ag is quite complicated. Depending on the applied stress and the temperature, a GB cracking phenomena can affect the creep rate and consequently contribute to the calculated value of creep activation energy. A tentative kinetic model of such a process reveals that the lifetime of a specimen may be controlled by a combination of one or more of the following diffusive processes: lattice- or GB, self- or hetero-diffusion. Work is now in progress on further analysis on GB crack nucleation and growth in order to verify the actual micromechanism and establish the activation energy that the process is controlled by.

ACKNOWLEDGMENT

This work was performed under the NSERC Industrial Research Fellowship to one of the authors (V.I.). The support received from Visteon Automotive Systems in Markham, Ontario, and Dearborn, MI, is acknowledged with thanks.

REFERENCES

1. J. Glazer, *Int. Mater. Rev.* 40 (2), 65 (1995).
2. V.I. Igoshev and J.I. Kleiman, *Creep Phenomena in Lead-Free Solders,* submitted to publication.
3. R. Darveaux and K. Banerji, *IEEE Trans. Components, Hybrids, and Manufacturing Technol.* 15 (6), 1013 (1992).
4. W. Yang, R.W. Messler, Jr. and L.E. Felton, *J. Electron. Mater.* 24 (10), 1465 (1995).
5. S.M. Lee, *Jpn. J. Appl. Phys.* Part 1, 35 (7), 3999 (1996).
6. W. Yang, R.W. Messler, Jr. and L.E. Felton, *J. Electron. Mater.* 23 (8), 765 (1994).
7. J. Friedel, *Dislocations,* (Oxford: Pergamon Press, 1964], p. 620.
8. C. Kaynak, A. Ankara and T.J. Baker, *Mater. Sci. Technol.* 12, 421 (1996).

---

[b]We assume here that the intermetallic particle acts as the most vulnerable microstructural component of the material as reported in Ref. 7.

[c]It should be kept in mind that Sn-3.5Ag alloy contains small particles of intermetallics, e.g., precipitates. Consequently, parameters of dislocation movements may be affected by these particles and the lifetime (cracking rate) can be controlled by the processes of bulk-, self-, or hetero-diffusion.

[d]The previously reported experimental data relevant to Sn-3.5Ag solder alloy[3,4] was obtained in the normalized stress range $(\sigma/E) = (1 \div 10) \times 10^{-4}$.

[e]Data presented in Ref. 8 on GB cracking of Pb-Sn eutectic solder indicates at a similar result, namely that the process starts at any early stage (~5% of lifetime) of cyclic loading.